HIGH TEMPERATURE OXIDATION OF EARLY TRANSITION METALS AND CARBIDES IN HYPERSONIC-RELEVANT CONDITIONS

Connor J. Stephens, Michael N. Richwine, Elizabeth J. Opila
University of Virginia
Department of Materials Science and Engineering

Abstract

The oxidation mechanisms and kinetics of Ta and TaC were observed via Joule heating in a custom resistive heating system. Oxidation was studied at 1300, 1400, and 1500°C from 2-10 minutes in a 1%O_2-Ar environment. Oxide sintering provides an essential protective mechanism in Ta where a dense oxide creates a diffusion barrier to oxidation, whereas in TaC, the porous nature of the oxide mitigates the effects of sintering. When sintering is active, TaC oxidizes more rapidly than Ta due to rapid oxygen ingress through the scale. In Ta, where solid-state diffusion plays a significant role, a phase transition in the oxide may play a secondary role in the overall effectiveness of the oxide as a diffusion barrier. A new system for evaluating oxidation in a dissociated oxygen environment is discussed.

Introduction

Hypersonic flight is typically designated as air/spacecraft travelling at Mach 5 or greater. During such flight, leading-edge (LE) components, such as nose caps and wing LEs, are often exposed to extremely high temperatures due to air friction, which in some cases can exceed 3000°C[1]. As hypersonic vehicle technology continues to develop, the need for materials that can withstand such environments continues to grow. Conventional high temperature structural materials have been SiC-based because of the exceptional protective behavior of SiO_2 against oxidation. However, SiO_2-based materials are limited by the melting point of SiO_2 (T_M=1727°C) and become nonprotective at T>1600°C due to SiO(g) formation[2]. Jacobson identified the limit set by SiO_2 which has become known as the "ultra-high" temperature regime[3]. A material that would enable flight at higher Mach number would ideally be mechanically strong, chemically stable, and lightweight above this temperature. The list of materials which do not melt in the extreme temperature range experienced by hypersonic LE components is very short, and a significant push for new, long-life, ultra-high temperature materials is underway.

a. Ultra-High Temperature Oxidation of Transition Metals and Carbides

Many of the current candidate materials for hypersonic LEs are comprised of early transition metal carbides (group IV, V, and VI metals)[1, 2, 4]. These carbides are noted for their high melting points and good strength retention at high temperatures. Unfortunately, these materials are especially prone to oxidation, as the formation of CO(g) during oxidation results in porous scale formation[5, 6]. The porous scale allows rapid ingress of oxygen to the base material and rapidly accelerates material degradation. The corresponding pure metals, lacking carbon, form much more dense scales which can help inhibit oxidation, though the significantly lower melting point of the metals restricts their high temperature use cases. In

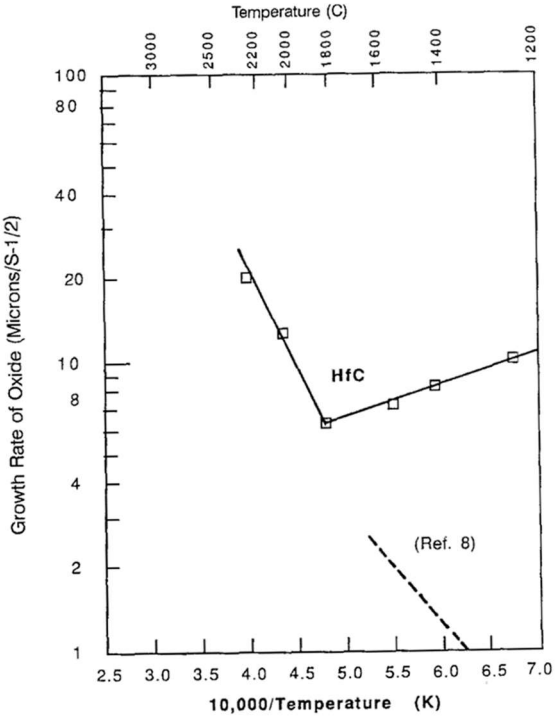

Figure 1: Comparison of oxidation rate of HfC and Hf (Ref 8. is Smeltzer and Simnad[10]. Reproduced from Courtright et al.[5]

addition to these differences, the metals tend to be less expensive and easier to manufacture. Thus, there is a great deal of interest in the differences between these material classes, and each has its own advantages and disadvantages.

Despite the great deal of interest in these materials and the extensive volume of literature regarding the oxidation of transition metals and carbides, the mechanisms which drive oxidation at high temperatures are poorly understood. There is also little to no kinetic oxidation data for the oxidation of these materials at temperatures higher than ~1300°C in high oxygen pressures[7-9]. Additionally, to the best of the author's knowledge, there are no known *direct comparisons* between the oxidation behavior of a metal and carbide in identical, repeatable conditions which may elucidate the overall role of carbon in the oxidation process. Courtright et al. measured the oxidation kinetics of HfC and compared the rate of oxidation to the rates published by Smeltzer and Simnad[10], shown in Figure 1[11]. This *indirect comparison* shows the rates of Hf vs HfC, though the exposure temperatures and experimental setups were very different.

The aim of this project is to address these knowledge gaps for several M vs MC_x systems (M = Ti, Zr, Hf, Ta). These materials were chosen from the group IV, V, and VI transition metals because they form solid oxides which are stable at temperatures greater than the melting point of SiO_2. The current work focuses on the Ta vs TaC system.

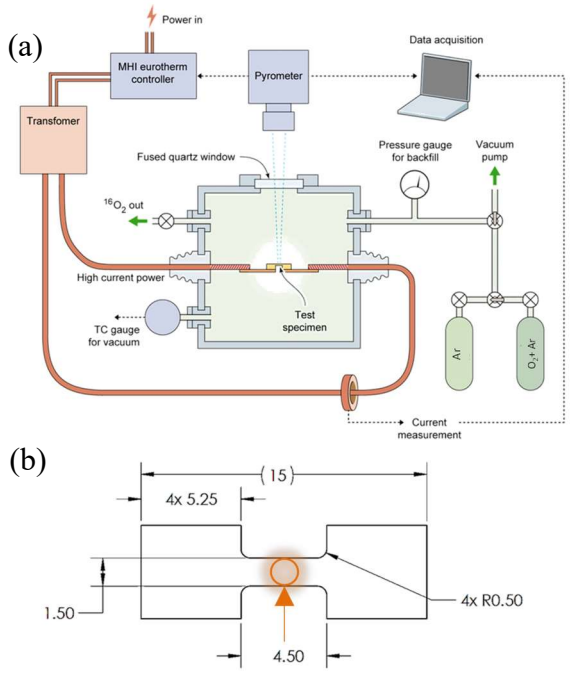

Figure 2: (a) Schematic of the RHS at the University of Virginia and (b) "dogbone" specimen dimensions used in the RHS.

b. Oxidation via Atomic Oxygen

Oxidation in ultra-high temperature environments is an extremely rapid process, but the hypersonic environment also contains dissociated oxygen, which may accelerate oxidation even further. At high Mach number speeds, shock waves at LEs coupled with ultra-high temperatures create a plasma-present environment conducive to the dissociation of molecular oxygen (MO) into atomic oxygen (AO). Typical oxidation involves the adsorption and dissociation of MO into AO on a surface prior to reacting with the base material. In a pre-dissociated environment, however, the activation energy barrier to oxidation may be lowered by the lack of bond dissociation. Thus, oxidation in AO is expected to be much more rapid than oxidation in MO. There are two common methods for generating AO: 1) microwave glow discharge plasmas – while cost effective, microwave plasmas often suffer from low radical fluence due to recombination at chamber walls[11]; and 2) arc-jets facilities /MESOX– these facilities are extremely expensive to operate and involve extremely high, indiscriminate jet flows which do not allow decoupling of the effects of temperature from AO[12]. Later in this work, the construction of a novel, cost-effective system for conducting high temperature oxidation experiments in a controlled AO environment will be discussed.

Experimental Methods

a. Custom Resistive Heating System

Oxidation was conducted using a custom resistive heating system (RHS), based on the design of Karlsdottir and Halloran[13] and modified by Shugart and Opila[14]. A schematic of the RHS is shown in Figure 2a. Samples are connected to Cu leads inside the chamber,

which can deliver over 100 Amps of current to the material. Because of the reduced cross section at the "hot zone" of the specimens, shown in orange in Figure 2b, the high current causes rapid Joule heating. Because the "hot zone" is not touching any other components, reactivity with experimental components is minimized. Current is delivered by a furnace control unit equipped with a Eurotherm controller (BPAN controller, Micropyretics Heaters International, Inc., Cincinnati, OH). The furnace controller receives temperature input from an emissivity-correcting pyrometer (Pyrofiber Lab, Pyrometer Instrument Co., Windsor, NJ) which adjusts the power output to match the desired temperature. Good temperature control can be maintained below 1800°C with an accuracy of roughly ±20°C at 1300°C and ±50°C at 1800°C. Pt foil is wrapped around the Cu leads, and Y-stabilized ZrO_2 (YSZ) padded alligator clips are used maintain good sample connection and to prevent reaction with the sample during heating.

b. Materials

A sheet of 0.635mm (0.025 in.) thick Ta (99.5% pure, metals basis) was sectioned via electrical discharge machining (Exothermics, Inc., Amherst, NH, USA) into a "dogbone" sample geometry, shown in Figure 2b. Large TaC pucks produced by hot isostatic pressing (Kurt J. Lesker Company, Pittsburg, PA) were diamond machined (Bomas Machining Specialties, Inc., Woburn, MA) into the dogbone geometry of 0.5mm (0.020 in) thick. Archimedes method indicated the TaC to be ~99.3% of theoretical density.

TaC has a large range of carbon stoichiometries which are possible, ranging from the hemicarbide (Ta_2C) to the monocarbide (TaC). Given the importance of the carbon content on oxidation, instrumental gas analysis (IGA) was used to verify the carbon content of the unoxidized carbide (Evans Analytical Group, Syracuse, NY). IGA indicated ~6.2wt% C, which correlates to ~50at% C (TaC_x, x=1).

High resolution transmission electron microscopy (HRTEM) and selected area electron diffraction (SAED) were used to probe the crystallinity of the carbide and to verify that the resulting carbon signal is all from the carbide phase and not from any free, amorphous carbon. Focused ion beam (FIB) milling was used to make thin foils of the TaC. The TEM results, shown in Figure 3, indicate a highly crystalline material with no amorphous free carbon. Thus, all oxidation results for TaC correspond with highly stoichiometric and phase pure TaC_x (x=1).

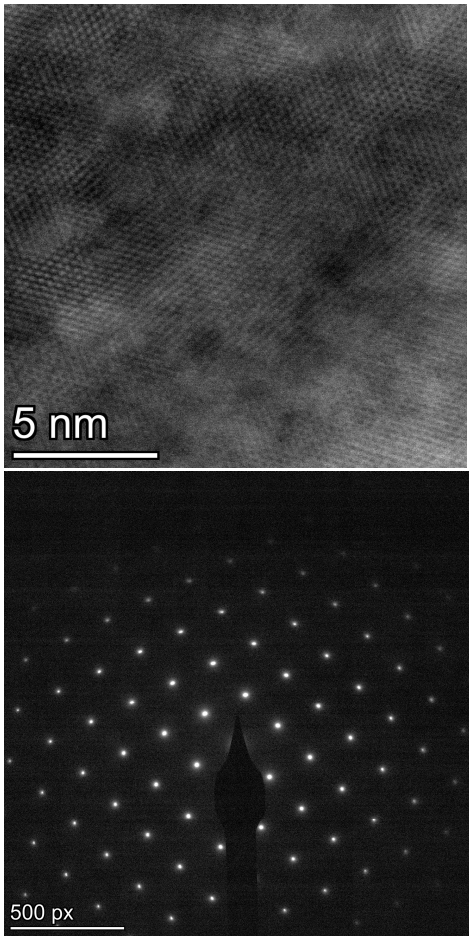

Figure 3: (a) HRTEM and (b) SAED pattern from an unoxidized TaC specimen.

c. Oxidation Experiments

Samples were loaded in the RHS and clipped to the conductive leads. The chamber was evacuated and backfilled with Ar until the pressure reached 50 mTorr or lower. Pure Ar was then introduced to the chamber until the system was at atmospheric pressure. Once at pressure, a gas exit valve was opened so that Ar flows continuously through the chamber. Gas flow was maintained at 950-1000 sccm for the duration of each experiment. Samples were heated to the desired temperature at 5°C/s in the pure Ar flow. Once at a stable temperature, the

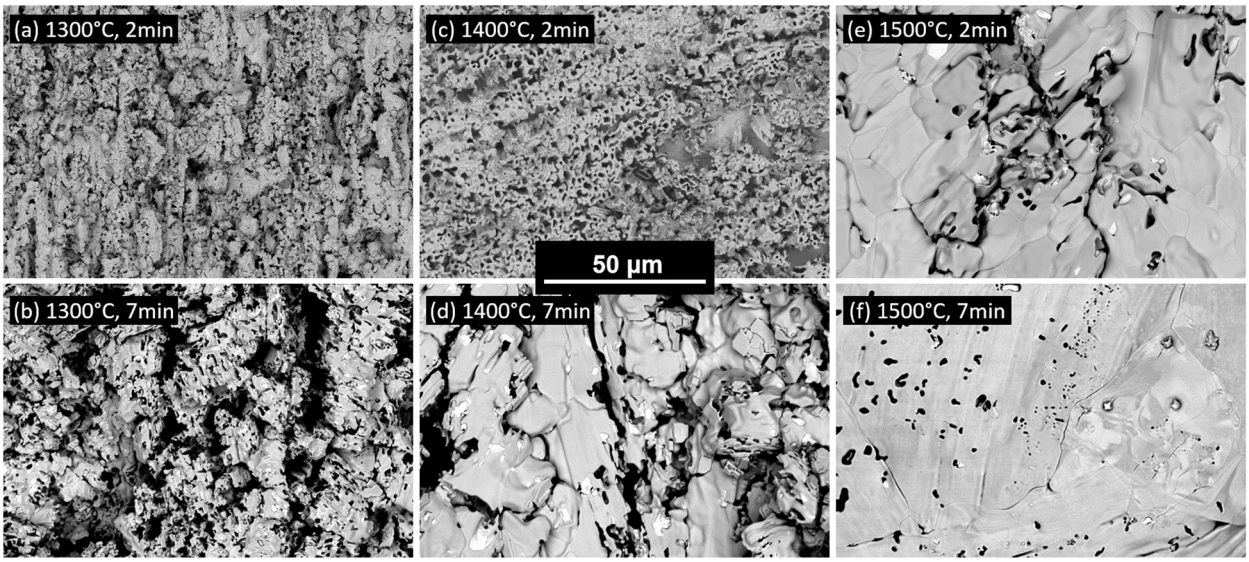

Figure 4: Plan view backscatter micrographs of Ta after (a,c,e) 2 min and (b,d,f) 7 min exposure times at (a-b) 1300°C, (c-d) 1400°C, and (e-f) 1500°C in 1%O_2-Ar.

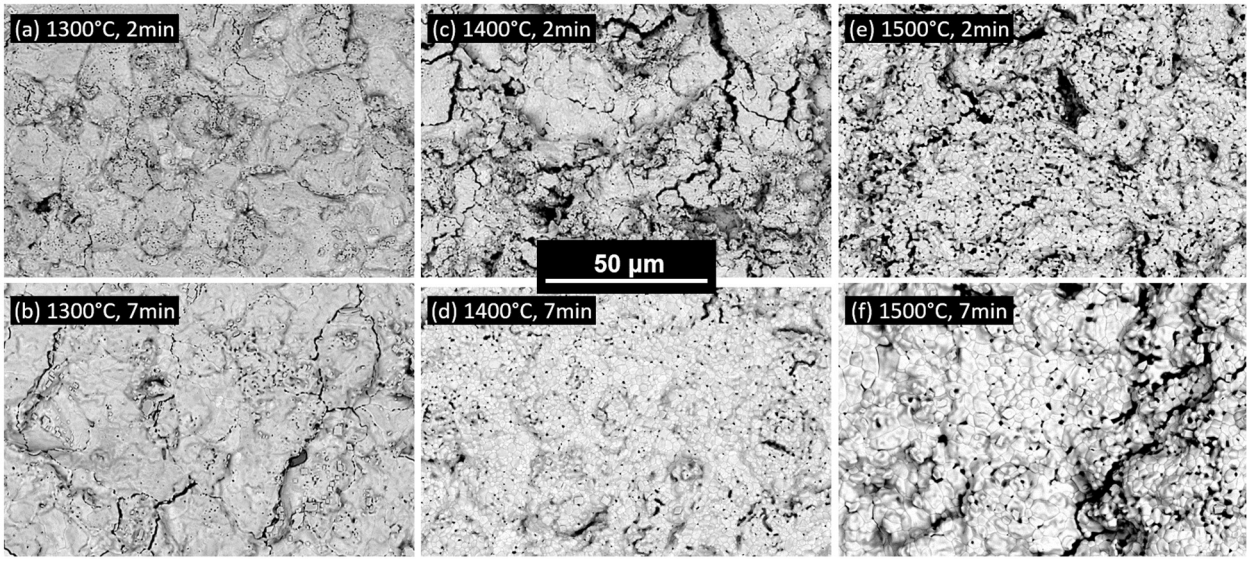

Figure 5: Plan view backscatter micrographs of TaC after (a,c,e) 2 min and (b,d,f) 7 min exposure times at (a-b) 1300°C, (c-d) 1400°C, and (e-f) 1500°C in 1%O_2-Ar.

gas was switched to a flowing 1% O_2-Ar mixture. Oxidation time started when oxygen was introduced to the system, and current flow was stopped at the end time of the experiment. When the current is stopped, the sample cools to near room temperature in only a few seconds.

Oxidation experiments were conducted at 1300, 1400, and 1500°C to fill in the gap of kinetic oxidation data for Ta and TaC. For each temperature, experiments were run between 2-10 minutes. In some cases, especially in the carbides, samples would break before the set end time. Because this stops current flow, these samples were still included in the data set with an end time at the time of fracture.

Samples were imaged using scanning electron microscopy (SEM) in 3 steps: 1) plan view, 2) fracture cross sections (pre-polish), and 3) polished cross sections. Samples were fractured close to the hot zone of the dogbone, then ground and polished to a 3µm fineness. Oxidation kinetics were determined from oxide thickness and base material recession.

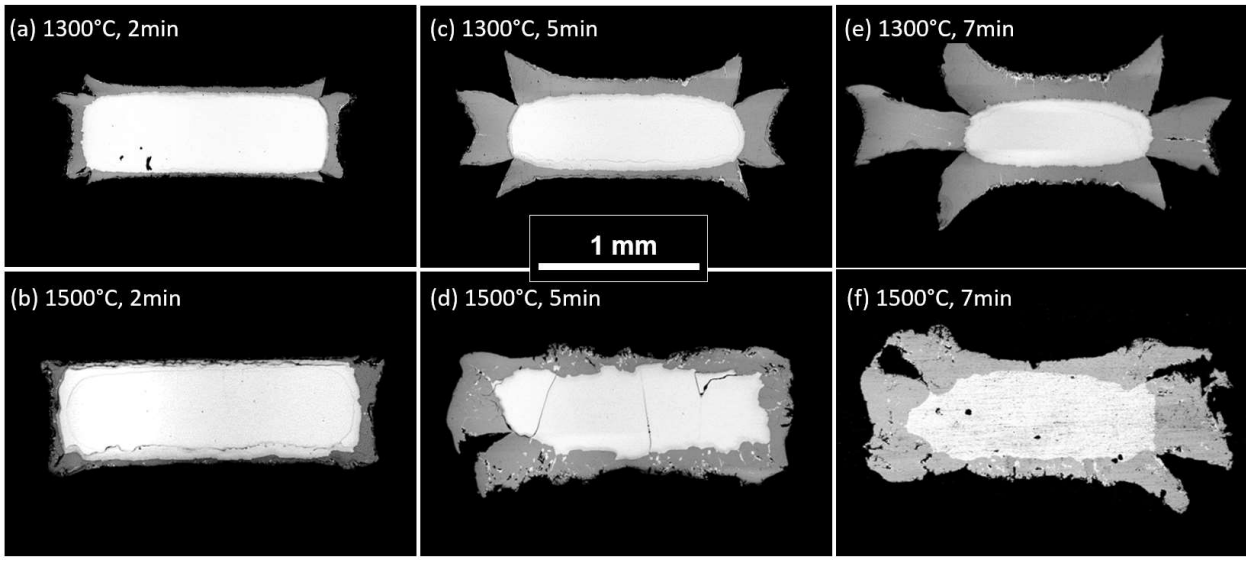

Figure 6: Cross section backscatter micrographs of polished Ta after (a-b) 2 min, (c-d) 5 min, and (e-f) 7 min exposure times at (a,c,e) 1300°C and (b,d,f) 1500°C in 1%O_2-Ar.

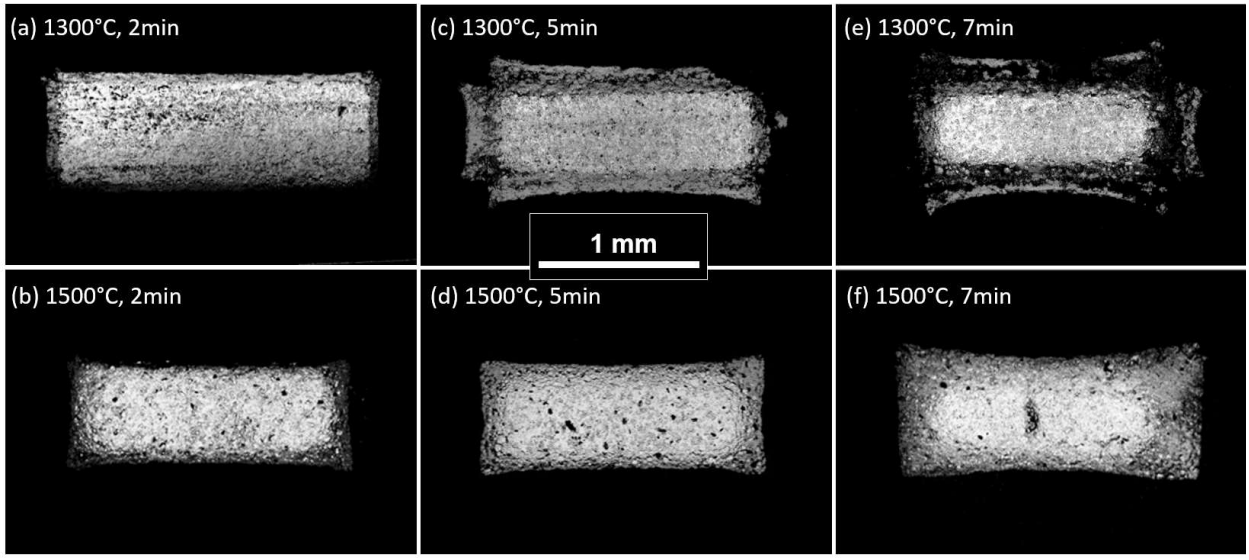

Figure 7: Cross section backscatter micrographs of polished TaC after (a-b) 2 min, (c-d) 5 min, and (e-f) 7 min exposure times at (a,c,e) 1300°C and (b,d,f) 1500°C in 1%O_2-Ar.

ImageJ [15] was used to measure the thickness of the bulk and the oxide at 10-20 points in the middle half of the polished cross section.

d. Diffraction Experiments

Ta_2O_5 undergoes a phase transformation at ~1360°C. Samples were analyzed post-oxidation using an X-ray diffractometer (XRD) equipped with a microfocus lens (Empyrean Diffractometer, Malvern Panalytical, Malvern, United Kingdom) to determine the product oxide phase assemblage. Microfocus XRD provides a relatively weak diffraction signal due to the small area of analysis. To better analyze the structure of the grown phases, two Ta samples were completely oxidized in a box furnace at 1300°C and 1450°C, then air quenched to simulate the end of an experiment in the RHS. The resulting oxides were ground to a powder and analyzed via XRD.

Results and Discussion

a. Oxide Morphology

A series of plan-view, post-oxidation micrographs for Ta and TaC are shown in Figure 4 and Figure 5, respectively. Both series

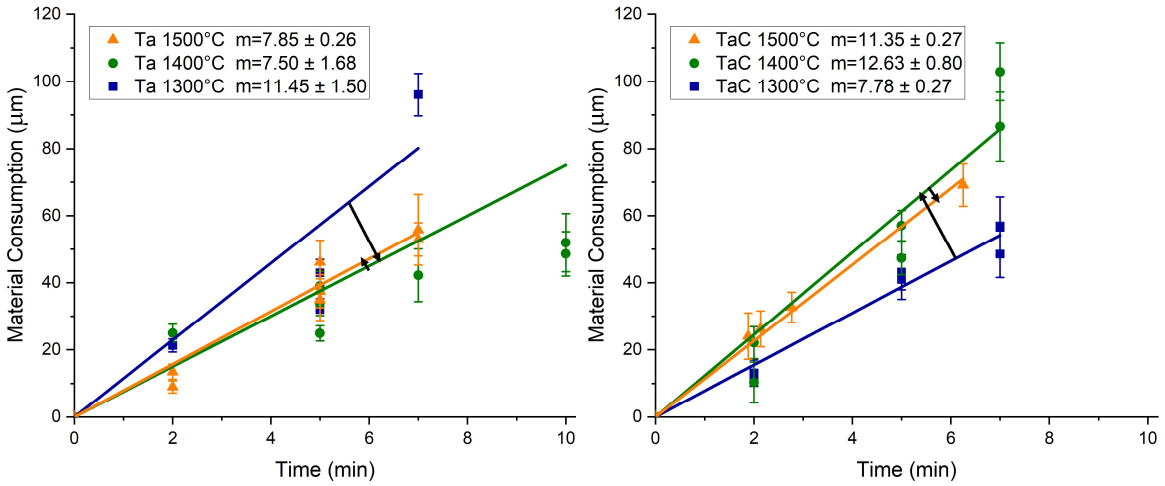

Figure 8: Comparison of the oxidation kinetics for Ta and TaC at 1300-1500°C in 1%O_2-Ar. The black arrows follow the direction of increasing temperature to highlight the abnormal behavior for Ta oxidation at 1300°C.

show oxidation at each temperature, at 2 minutes (top) and 7 minutes (bottom). Each material shows a similar trend with temperature and time, with a few notable differences. The surface of the oxide formed on Ta at 1300°C has a few wide-spread openings which become more open as time progresses. At 1400°C, this trend is reversed, with many of the small oxide grains coalesce and form plate-like structures which close off the oxide. This trend also persists at 1500°C but happens faster than at 1400°C. Interestingly, a large volume of unreacted Ta metal can be found throughout the oxide, both on the surface (bright phase in Figure 4 b, d, e, f), as well as within the oxide, shown in Figure 9b. Ta is found on the surface, in fracture, and in polished sections, and so is not an artifact of sample preparation. The exact mechanism for this behavior requires further study.

There is also a change in oxide morphology formed on TaC from 1300°C to 1400°C, though it is different from the metal. At 1300°C, microcracking develops with time on the surface of the oxide. At 1400°C, the oxide forms plate-like structures, but the grains tend to form in well-defined, rounded shapes separated by voids and pores. As time progresses, these rounded grains coalesce and the pores either disappear or merge and are found on the grain boundaries. This progression in microstructure is highly indicative of sintering in the oxide.

This behavior is not consistent with the Ta metal, despite the identical reaction products and experimental conditions. As was previously established, the presence of C and the formation of CO(g) during oxidation creates additional surface area by forming a porous oxide. Because sintering is a diffusion-based process driven by the minimization of surface area, the increase in surface energy likely creates greater driving forces for sintering.

Differences in oxide morphology can be seen more easily in cross section. Fracture (top) and polished (bottom) cross sections post-oxidation at 1300°C (left) and 1400°C (right) for Ta and TaC are shown in Figure 6 and Figure 7, respectively. The oxide formed on Ta is dense, continuous and exhibits columnar growth normal to the substrate surface, evident from the fracture surface. The oxide formed on TaC is very porous and has large grains of TaC embedded in the oxide due to intergranular oxidation. There does not appear to be a preferred growth direction, likely because the oxide is broken up during growth from CO(g) production.

The oxide forms a ‘Maltese Cross’ on both materials due to the large molar volume change during oxidation (Pilling-Bedworth Ratio (PBR) of Ta/Ta_2O_5 ~2.5; TaC/Ta_2O_5 ~2). At 1300°C, this shape is sharp and well defined. At 1400 and 1500°C, the corners of the cross have collapsed. This is also evidence of oxide sintering, which appears to play a major role in the overall oxidation behavior of Ta and TaC.

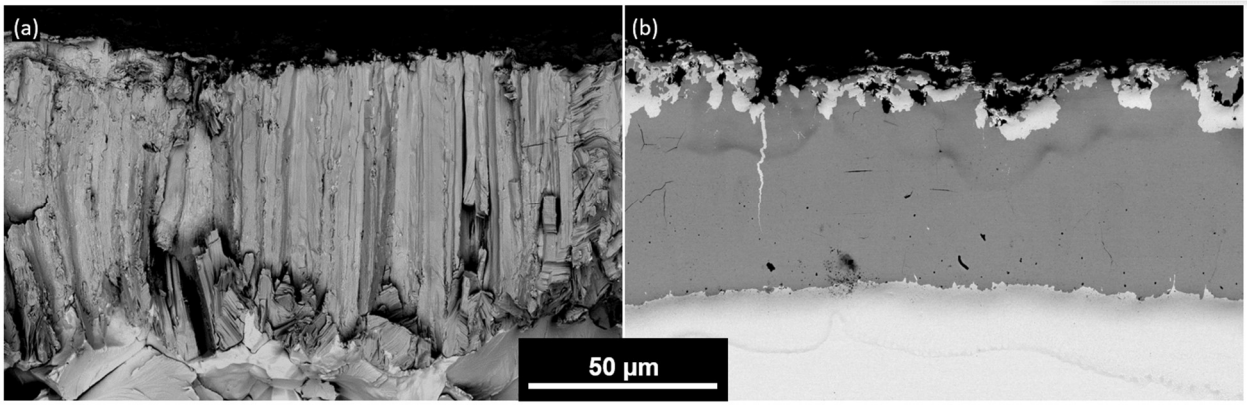

Figure 9: Cross section backscatter micrograph of (a) fractured and (b) polished Ta, oxidized at 1300°C for 7 min in 1%O_2-Ar (same sample). Note the columnar microstructure in the fractured oxide, as well as the unreacted Ta metal on the surface of the oxide in the polished section.

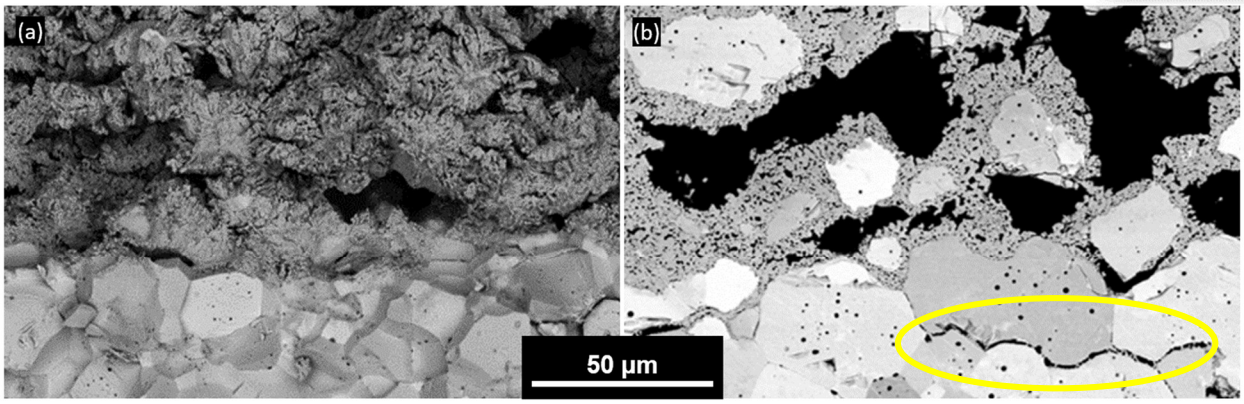

Figure 10: Cross section backscatter micrograph of (a) fractured and (b) polished TaC, oxidized at 1400°C for 5 min in 1%O_2-Ar (same sample). The yellow circle is highlighting oxides forming inside a grain boundary, leading to the grain lift out seen in the oxide.

b. Oxidation Kinetics and Mechanisms

Figure 8 shows a comparison of the material recession for Ta and TaC resulting from oxidation. The oxidation rate of Ta is of significant note and decreases dramatically with an increase in temperature from 1300 to 1400°C, but remains relatively constant from 1400 to 1500°C. TaC, on the other hand, shows an increase in oxidation rate from 1300-1400°C. Because the porous oxide on TaC allows rapid ingress of oxygen to the substrate, the increase in rate is likely due to gas-phase-diffusion limited transport through the oxide scale. Given that the oxide phase formed on Ta and TaC should be the same Ta_2O_5 phase in identical experimental conditions, this implies that the reason for the decrease in oxidation rate for Ta is governed by oxide morphology rather than chemistry. Oxygen transport to the substrate through the oxide on Ta is governed by solid-state diffusion, while gas-phase diffusion governs transport through the oxide on TaC. Sintering of the Ta_2O_5 scale at temperatures of 1400°C and above appears to enhance the protective capabilities of the oxide scale formed on Ta, while the porous scale on TaC results in a greater oxidation rate, despite the apparently greater driving force for sintering.

The resulting oxide morphology offers many possible pathways by which oxygen might diffuse towards the base materials. The Maltese cross, which splits due to growth stresses during oxidation, creates points at the corners where the oxide is very thin. These points, which exist only when sintering does not occur, are very likely the source of the rapid oxidation rate in Ta at 1300°C. In contrast, at 1400 and 1500°C, sintering may be the cause for these points closing, forcing oxygen to diffuse across the full thickness of the oxide. The columnar structure visible in the fracture

cross section may allow rapid grain boundary ingress of oxygen towards the metal surface when fast access to the corners of the metal is unavailable. This grain boundary diffusion is still significantly slower than the attack at the corners, and thus, the oxidation rate decreases when sintering is active.

Oxide sintering does not play as significant of a role for TaC, as oxygen diffuses rapidly through scale regardless of the sample corners. The magnitude of the change in TaC oxidation rate from 1400 to 1500°C is small and not distinguishable within experimental error. The change from 1300 to 1400°C, however, is much more significant. This is likely because sintering still prevents rapid oxygen ingress at the corners of the samples, and oxygen now must migrate via gas-phase diffusion across the thickness of the oxide. As gas-phase diffusion is orders of magnitude faster than solid-state diffusion and has a weak temperature dependence, the result is an increase in oxidation rate from 1300 to 1400°C.

It could be argued that the temperature dependence of oxidation should only be compared in regions where the sintering behavior is the same, such as between 1400 and 1500°C. This is especially true for small samples, where the corners play a major role in sintering and comprise a significant part of the sample surface area.

Oxidation appears to preferentially attack the grain boundaries in TaC, as shown in Figure 10. The large molar volume change from carbide (PBR ~2) to oxide appears to lift the grains out of place while oxidation continues beneath them, thus large carbide grains are present in the oxide. Ta appears to oxidize through the metal grains rather than attacking grain boundaries. However, there is a large difference in average grain size between the metal and carbide which may be account for this observation. Further investigation is underway to evaluate the effects of grain size on oxidation rate.

c. Oxide Phase Transformation

The Ta_2O_5 phase transformation at 1360°C may also play a role in the changing oxidation rate. The crystal structure of Ta_2O_5 is relatively well studied; however, there is still uncertainty regarding its high temperature crystal structure[16-19]. The low-temperature form, L-Ta_2O_5, is orthorhombic and is

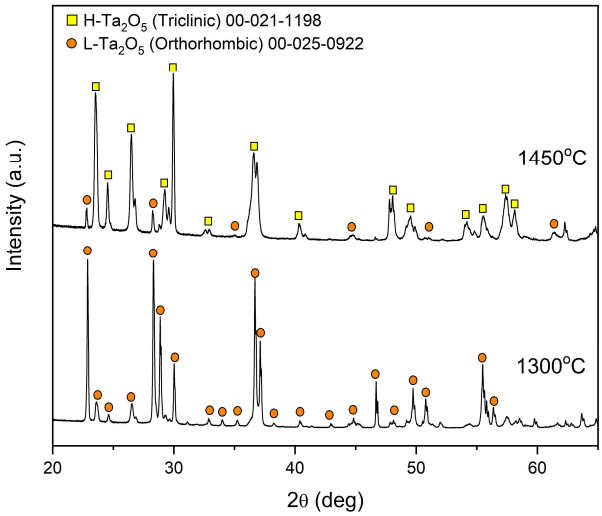

Figure 11: XRD patterns from Ta samples completely oxidized in a stagnant air box furnace and quenched.

incommensurately modulated in the *b*-direction[20-22]. At 1360°C, the oxide transforms to a tetragonal phase, H-Ta_2O_5. Due to the sluggish and reversible nature of the phase transformation, H-Ta_2O_5 cannot be stabilized at room temperature, making it very difficult to determine its equilibrium structure. Quenching the high temperature phase causes the oxide to transform through a series of metastable polymorphs during cooling, ending as a triclinic crystal[23]. Stephenson and Roth stabilized the structure by doping the oxide with ~2wt% Sc_2O_3[24], though there is still no high-quality diffraction data available for undoped H-Ta_2O_5.

The diffraction patterns from the two completely oxidized samples are shown in Figure 11. As expected, H-Ta_2O_5 was not found in either sample. The sample oxidized below the phase transformation temperature formed exclusively orthorhombic L-Ta_2O_5, while the sample oxidized above the phase transformation temperature formed a triclinic phase and minor amounts of L-Ta_2O_5. This is consistent with the current understanding of the Ta_2O_5 phase transformation and implies that H-Ta_2O_5 is the formed phase at high temperatures. Upon cooling, some oxide transforms back to L-Ta_2O_5, but the primary transformation follows the metastable path to the triclinic phase. Understanding the role of the Ta_2O_5 phase transformation in oxidation will require significant additional study.

Conclusions

The oxidation of Ta and TaC were compared in identical conditions for the first time to understand the role of carbon on the oxidation mechanism. Experiments were conducted using a custom resistive heating system for times of 2-10 minutes at temperatures of 1300, 1400, and 1500°C in a 1%O_2-Ar environment. Oxide morphology was characterized using scanning electron microscopy. Oxide phase assemblage was observed with micro-X-ray diffraction. The kinetics of oxidation were determined from substrate recession measurements. Oxide sintering plays a significant role in the oxidation kinetics of Ta and TaC. At 1400 and 1500°C, sintering of the oxide seals off fast-oxidation pathways through the oxide formed on Ta causing a decrease in oxidation rate. In TaC, the porous nature of the oxide enables rapid oxygen ingress at all temperatures, regardless of if sintering occurs.

Construction of M-RHS

It is necessary to consider high-temperature oxidation in an AO environment to evaluate a material's effectiveness for hypersonic application. The available methods which can create high-fluence AO environments at high temperatures (arc-jets, MESOX) are very expensive to operate. A new, cost-effective method of generating AO is needed to rapidly evaluate a high volume of candidate materials in an AO environment. As part of this work, a new RHS was constructed with the added addition of a microplasma (MP) capillary jet. This new system is referred to as the Microplasma Resistive Heating System (M-RHS).

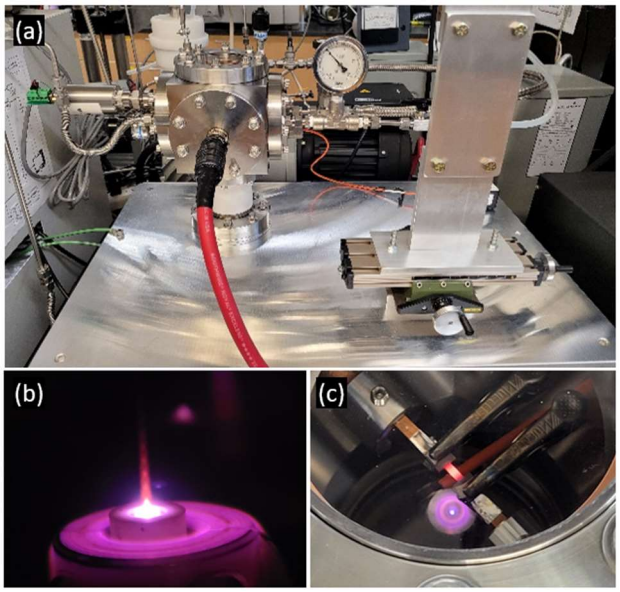

Figure 12: (a) Fully constructed chamber and stand of the M-RHS; (b) active MP jet flowing 1%O_2-Ar gas; (c) the M-RHS heating a Hf dogbone in an O-Ar plasma.

The key characteristics of a MP are 1) high-pressure stability (~10 Torr magnitudes); 2) a non-Maxwellian electron energy distribution function with a high energy tail capable of dissociating molecular gases; and 3) non-equilibrium thermodynamics, where the large surface-area to volume ratio of the plasma jet allows for a 'cold plasma' ($T<100°C$)[25]. The high temperature oxidation kinetics in AO can be measured by utilizing a MP in conjunction with a RHS. Additionally, the effects of the AO plasma can be isolated from any coupled effects during high temperature oxidation because the plasma is "cold".

The M-RHS has been fully constructed and is shown in Figure 12. The design is very similar to the RHS, with the major difference being the incorporation of a MP capillary on the unused bottom flange. The total cost for construction is approximately equal to the hourly operation rate for other conventional high temperature AO generation techniques.

Acknowledgements

The author would like to thank: Mr. Steve DiPietro and Exothermics, Inc. for providing the Ta; Dr. H. Heinrich for assisting with the FIB, HRTEM, and SAED; Dr. M. Gordon for helpful discussion and advice in constructing the microplasma system; Mr. M. Richwine for unenumerable help; and Dr. E. Opila for her guidance and patience during this process.

Use of the Quanta 650 FEG-SEM and the Empyrean Diffractometer was possible through the University of Virginia Nanoscale Materials Characterization Facility (NMCF).

This project was funded by the Air Force Office of Scientific Research (AFOSR). Funding for the construction of the M-RHS was provided by the AFOSR Defense University Research Instrumentation Program (DURIP). Additional resources were provided by the Virginia Space Grant Consortium (VSGC) Graduate Student Fellowship Program.

References

[1] Wuchina, E., Opila, E., Opeka, M., Fahrenholtz, B., Talmy, I. (2007). The Electrochemical Society Interface,16(4), 30.

[2] M. M. Opeka, I. G. Talmy, and J. A. Zaykoski, *J Mater Sci*, vol. 39, no. 19, pp. 5887–5904, 2004.

[3] N. S. Jacobson, *Journal of the American Ceramic Society*, 76: 3-28, 1993

[4] T. A. Parthasarathy, R. A. Rapp, M. M. Opeka, and R. J. Kerans, *Acta Mater*, vol. 55, no. 17, pp. 5999–6010, 2007

[5] E. L. Courtright, J. T. Prater, G. R. Holcomb, G. R. St. Pierre, and R. A. Rapp, *Oxidation of Metals*, vol. 36, no. 5–6, pp. 423–437, 1991

[6] G. R. Holcomb and G. R. S. Pierre, *Oxidation of Metals*, vol. 40, no. 1–2, pp. 109–118, 1993

[7] P. Kofstad, *J Electrochem Soc*, vol. 110, no. 6, p. 491, 1963

[8] P. Kofstad, *Journal of the Less Common Metals*, vol. 5, no. 2, pp. 158–170, Apr. 1963

[9] P. Kofstad, *Journal of The Less-Common Metals*, vol. 7, no. 4, pp. 241–266, 1964

[10] W. W. Smeltzer and M. T. Simnad, *Acta Metallurgica*, vol. 5, no. 6, pp. 328–334, 1957

[11] G. Primc, R. Zaplotnik, A. Vesel, and M. Mozetic, *AIP Adv*, vol. 1, no. 2, 2011

[12] F. Monteverde, R. Savino, M. D. S. Fumo, and A. Di Maso, *J Eur Ceram Soc*, vol. 30, no. 11, pp. 2313–2321, Aug. 2010

[13] S. N. Karlsdottir and J. W. Halloran, *Journal of the American Ceramic Society*, vol. 90, no. 10, pp. 3233–3238, 2007

[14] K. Shugart, B. Patterson, D. Lichtman, S. Liu, and E. Opila, *Journal of the American Ceramic Society*, vol. 97, no. 7, pp. 2279–2285, 2014

[15] Schneider, C. A., Rasband, W. S., & Eliceiri, K. W., *Nature Methods*, *9*(7), 671–675, 2012

[16] N. C. Stephenson and R. S. Roth, *J Solid State Chem*, vol. 18, no. 2, pp. 145–153, 1970

[17] D. Makovec, J. M. Zuo, R. Twesten, and D. A. Payne, *J Solid State Chem*, vol. 179, no. 6, pp. 1782–1791, 2006

[18] G. L. Brennecka, D. A. Payne, P. Sarin, J. M. Zuo, W. M. Kriven, and H. Hellwig, *Journal of the American Ceramic Society*, vol. 90, no. 9, pp. 2947–2953, 2007

[19] X. Q. Liu, X. D. Han, Z. Zhang, L. F. Ji, and Y. J. Jiang, *Acta Mater*, vol. 55, no. 7, pp. 2385–2396, 2007

[20] N. C. Stephenson and R. S. Roth, *Acta Crystallogr B*, vol. 27, no. 5, pp. 1037–1044, 1971

[21] I. E. Grey, W. G. Mumme, and R. S. Roth, *J Solid State Chem*, vol. 178, no. 11, pp. 3308–3314, 2005

[22] S. Schmid, R. L. Withers, and J. G. Thompson, *J Solid State Chem*, vol. 99, no. 2, pp. 226–242, 1992

[23] J. L. Waring and R. S. Roth, *J Res Natl Bur Stand A Phys Chem*, vol. 72A, no. 2, p. 175, 1968

[24] R. S. Roth, J. L. Waring, and W. S. Brower, *J Res Natl Bur Stand A Phys Chem*, vol. 74A, no. 4, p. 477, 1970

[25] T. L. Koh, E. C. O'Hara, and M. J. Gordon, *Nanotechnology*, vol. 23, no. 42, 2012